


 Cite this: *Chem. Commun.*, 2019, 55, 6894

 Received 11th April 2019,  
 Accepted 17th May 2019

DOI: 10.1039/c9cc02823d

rsc.li/chemcomm

## A uranium capture strategy based on self-assembly in a hydroxyl-functionalized ionic liquid extraction system†

 Baihua Chen,<sup>a</sup> Kaige Wu,<sup>b</sup> Yanqiu Yang,<sup>ib</sup> Ning Wang,<sup>a</sup> Yi Liu,<sup>a</sup> Shuanglin Hu,<sup>ib</sup> Jing Wang,<sup>a</sup> Jun Wen,<sup>a</sup> Sheng Hu,<sup>a</sup> Qingde Chen,<sup>ib</sup> Xinghai Shen<sup>\*b</sup> and Shuming Peng<sup>ib</sup> <sup>\*a</sup>

**A novel and efficient uranium capture strategy based on self-assembly is developed in an ionic liquid extraction system, by which the one-step separation and solidification of uranium are realized. This not only provides a promising method for separating metal ions but also promotes the development of a supramolecular assembly both in mechanism and application.**

Nuclear energy with low carbon emission is regarded as one of the most promising solutions to the world's growing need for clean energy.<sup>1</sup> Extensive studies have been focused on the separation and purification of uranium,<sup>2–6</sup> the actual fuel for the production of nuclear energy. Solvent extraction is the most practically mature technology for this purpose. However, the drawbacks of this traditional method are back extraction for concentrating metal ions and treatment of organic wastes, especially radioactive wastes. Therefore, the simplification of the separation process has attracted significant attention. The self-assembly of metal ions and ligands in organic phases is found in many extraction systems,<sup>7,8</sup> but these assemblies stop aggregation at microscopic or mesoscopic scales. If they can further aggregate to the macroscopic scale, an easy-to-separate target could be obtained. Self-assembly at all scales, being essential as a unique methodology to fabricate bulk materials by bridging self-assembly at the molecular level and at the macroscopic scale, has made considerable developments in supramolecular chemistry.<sup>9–12</sup> The realization of self-assembly at all scales, a process with numerous interactive groups associating through non-covalent interactions in a multivalent manner, must meet two important requirements: one being intermolecular interactions and the other being driving forces which can propel the building blocks to move towards

each other and reach a nanoscale distance for sufficient interaction.<sup>9</sup>

Several kinds of intermolecular interactions such as hydrogen bonding, host-guest molecular recognition, electrostatic interaction, metal coordination, magnetic interactions, and DNA hybridization have been developed to realize self-assembly,<sup>13</sup> most of which are commonly found in extraction systems. Meanwhile, it was found that the combination of Marangoni-driven self-propulsion and molecular interaction could successfully induce collisions and the macroscopic supramolecular assembly.<sup>14</sup> Nonetheless, the Marangoni effect due to the surface tension gradient<sup>15</sup> usually lasts for a relatively short time, which leads to a poor assembly efficiency.<sup>14</sup> If the Marangoni effect is established in carefully designed extraction systems and is able to offer driving forces continuously, the spontaneous formation of macroscopic assemblies can be realized, which may provide not only a unique extraction strategy but also novel insights into the mechanism of supramolecular assembly.

Ionic liquids (ILs) as an eco-friendly and innovative class of solvents have been extensively applied in the study of extraction and separation,<sup>1,16–18</sup> acting as organic solvents and meanwhile participating in the formation of an extraction complex. In particular, the extraction systems based on ILs composed of the imidazolium cation and the bis(trifluoromethylsulfonyl) anion exhibit excellent extraction efficiency.<sup>1,19,20</sup> Very recently, a hydroxyl-functionalized IL, *e.g.* [HEMIm][NTf<sub>2</sub>] attracted our attention because of its surfactant-like behaviours and different surface tensions compared with similar ILs without hydroxyl groups,<sup>21</sup> which is crucial to trigger the Marangoni effect. We intuitively believe that the introduction of [HEMIm][NTf<sub>2</sub>] in the extraction system may induce Marangoni interactions at the aqueous-IL interface, by which self-assembly processes may be driven.

Herein, we developed a novel extraction strategy for uranium based on self-assembly with a hydroxyl-functionalized IL. CMPO is selected as the ligand to bind uranyl ions in the designed extraction system. Two solutions of equal volumes, CMPO in [HEMIm][NTf<sub>2</sub>] and uranyl in HNO<sub>3</sub>, were mixed together to

<sup>a</sup> Institute of Nuclear Physics and Chemistry, China Academy of Engineering Physics, Sichuan, Mianyang, 621999, P. R. China. E-mail: pengshuming@caep.cn

<sup>b</sup> Beijing National Laboratory for Molecular Sciences (BNLMS), Fundamental Science on Radiochemistry and Radiation Chemistry Laboratory, Center for Applied Physics and Technology, College of Chemistry and Molecular Engineering Peking University, Beijing, 100871, P. R. China. E-mail: xshen@pku.edu.cn

† Electronic supplementary information (ESI) available. See DOI: 10.1039/c9cc02823d



Fig. 1 Self-assembly of the uranium-rich SA sample.

perform the extraction experiment (see the ESI† for details). Interestingly, a macroscopic solid phase was formed at the aqueous–IL interface through self-assembly, which is drastically different from that of the traditional extraction process (Fig. 1 and Supplementary Movie, ESI†). The solid phase was then confirmed to be uranium-rich by ICP-OES and could be easily captured using a tweezer. Thus, the one-step extraction and solidification of uranyl ions from aqueous solution were realized without back extraction and free of the radioactive waste (the uranium residual in the aqueous phase is below 0.05% of the initial and the reusability of the IL is examined to be excellent; see the following section). A possible explanation for the formation of the macro assembly is discussed, in the hope of offering a simple and convenient uranyl recovery method and an advancement of supramolecular assembly in theory and in application.

To obtain the morphological, compositional and structural information of the uranium-rich self-assembly sample (the SA sample), various characterization techniques were utilized. First, the sample was cut into pieces and scanned by SEM (Fig. 2a). The EDS mapping of uranium (Fig. 2B) as well as carbon, fluorine, oxygen, phosphorus and sulphur (Fig. S3, ESI†) showed that all these elements were uniformly distributed on the sample. In the extraction system used, CMPO and [HEMIm][NTf<sub>2</sub>] are the only possible sources of these main group elements, hence the ligand

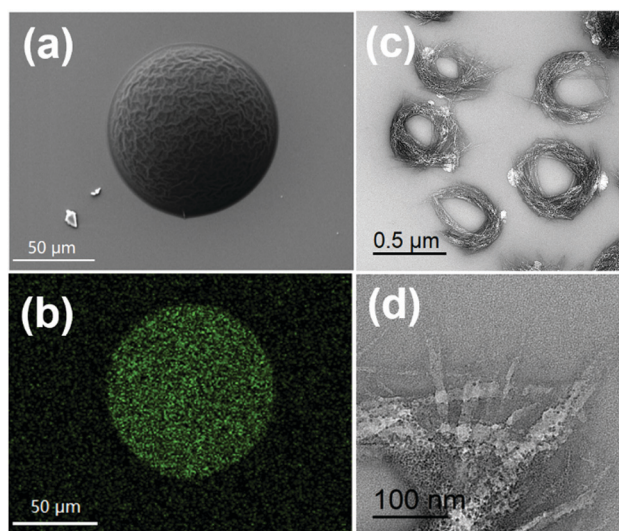


Fig. 2 The morphological characterizations of the disrupted SA sample. (a) The SEM image of the disrupted sample, (b) EDS mapping of the uranium element and (c) and (d) TEM images.

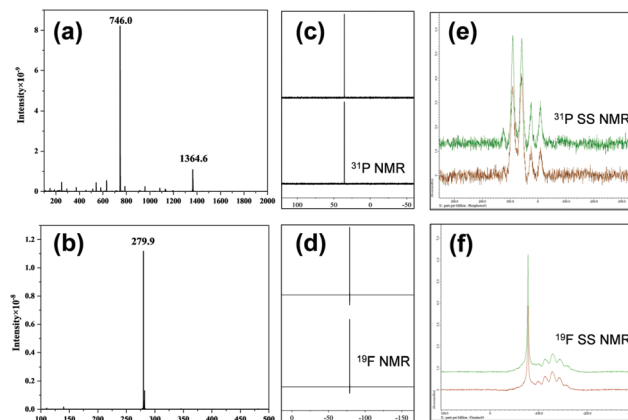


Fig. 3 The spectroscopic analyses of the SA sample. (a) Mass spectra of the SA sample in positive mode. (b) Mass spectra of the SA sample in negative mode. (c) <sup>31</sup>P NMR spectra of the *d*<sub>6</sub>-DMSO dissolved UO<sub>2</sub>(CMPO)<sub>3</sub>(NO<sub>3</sub>)<sub>2</sub> (upper curve) and the SA sample (lower curve). (d) <sup>19</sup>F NMR spectra of [HEMIm][NTf<sub>2</sub>] (upper curve) and the *d*<sub>6</sub>-DMSO dissolved SA sample (lower curve). (e) Solid state NMR spectra of <sup>31</sup>P for the SA sample (green curve) and synthesized UO<sub>2</sub>(CMPO)<sub>3</sub>(NTf<sub>2</sub>)<sub>2</sub> (brown curve). (f) Solid state NMR spectra of <sup>19</sup>F for the SA sample (green curve) and synthesized UO<sub>2</sub>(CMPO)<sub>3</sub>(NTf<sub>2</sub>)<sub>2</sub> (brown curve).

and the IL should both participate in the formation of the SA sample. When the SA sample was treated with NaOH solutions (the self-assembly process is pH-responsive and reversible, see Fig. S1, ESI†) and characterized by TEM, some nest-like structures constructed with nanowires appeared (Fig. 2c, d, and Fig. S2, ESI†), suggesting that the SA sample might consist of such nanowires.

More evidence was obtained from the mass spectrometry results (Fig. 3a and b) indicating that the peak at *m/z* 746.0 in positive mode was attributed to UO<sub>2</sub>(CMPO)<sub>3</sub><sup>2+</sup> and the peak at *m/z* 279.9 in negative mode was assigned to NTf<sub>2</sub><sup>-</sup>. The <sup>31</sup>P and <sup>19</sup>F NMR spectra of the *d*<sub>6</sub>-DMSO dissolved SA sample further confirmed the existence of UO<sub>2</sub>(CMPO)<sub>3</sub><sup>2+</sup> and NTf<sub>2</sub><sup>-</sup> in the composition, as the chemical shift of P is identical to that of the synthesized UO<sub>2</sub>(CMPO)<sub>3</sub>(NO<sub>3</sub>)<sub>2</sub>, while the SA sample and [HEMIm][NTf<sub>2</sub>] have the same chemical shift as that of F (Fig. 3c and d). As shown in the related infrared spectra (Fig. S4, ESI†), absorptions corresponding to UO<sub>2</sub>(CMPO)<sub>3</sub><sup>2+</sup> and [HEMIm][NTf<sub>2</sub>] were found but no peak was centered around 1338 cm<sup>-1</sup> (the characteristic absorption of NO<sub>3</sub><sup>-</sup>), indicating the absence of NO<sub>3</sub><sup>-</sup> in the SA sample. To further verify the unnecessary NO<sub>3</sub><sup>-</sup> in the self-assembly process, ClO<sub>4</sub><sup>-</sup> was used in this extraction system instead of NO<sub>3</sub><sup>-</sup>, and then the SA sample was also obtained. The TG curve together with the pyrolysis FTIR spectra (Fig. S5, ESI†) revealed that no structural water was contained. Furthermore, the elemental analysis results (Table S1, ESI†) demonstrated that the composition of the SA sample was in close agreement with that of [UO<sub>2</sub>(CMPO)<sub>3</sub>]<sup>2+</sup>: [HEMIm]<sup>+</sup>: [NTf<sub>2</sub>]<sup>-</sup> = 3 : 1 : 7 molar ratio.

Wide angle X-ray scattering (WAXS) was conducted to test the periodicity of the sample. The WAXS patterns (Fig. S6, ESI†) indicate that an ordered structure is formed in the SA sample and the calculated periodic order is 1.42 nm, matching with the

theoretically calculated radius of the  $\text{UO}_2(\text{CMPO})_3^{2+}$  complex (Fig. S7, ESI<sup>†</sup>). To test whether the coordination environment of uranyl in the SA sample changes in regards to  $\text{UO}_2(\text{CMPO})_3(\text{NTf}_2)_2$ , the solid state NMR spectra of  $^{31}\text{P}$  (Fig. 3e) and  $^{19}\text{F}$  (Fig. 3f) for both samples were recorded for comparison. The almost identical feature proves that the coordination environment of CMPO and  $\text{NTf}_2^-$  in the SA sample is the same as that in the synthesized  $\text{UO}_2(\text{CMPO})_3(\text{NTf}_2)_2$ . On the basis of given evidence, the SA sample was deduced to be the macroscopic assembly of  $\{[\text{UO}_2(\text{CMPO})_3]_3[\text{HEMIm}]\}[\text{NTf}_2]_7$ .

To investigate the formation mechanism of the SA sample, additional experiments were conducted under the same conditions in analogous ILs without hydroxyl functional groups in the cationic moieties, such as  $[\text{C}_1\text{C}_2\text{Im}][\text{NTf}_2]$ ,  $[\text{C}_1\text{C}_4\text{Im}][\text{NTf}_2]$ ,  $[\text{C}_1\text{C}_6\text{Im}][\text{NTf}_2]$  and  $[\text{C}_1\text{C}_8\text{Im}][\text{NTf}_2]$ . The SA sample formation was not observed at the aqueous–IL interface in all the cases, demonstrating the significance of hydroxyl functional groups. Dynamic light scattering (DLS) was performed to further support this deduction on the mesoscopic scale.  $\text{UO}_2(\text{CMPO})_3(\text{NTf}_2)_2$  was synthesized and carefully dissolved in small amounts in  $[\text{HEMIm}][\text{NTf}_2]$  and  $[\text{C}_1\text{C}_2\text{Im}][\text{NTf}_2]$ , respectively, to maintain a homogeneous phase (see the ESI<sup>†</sup> and Fig. S8). Only in  $[\text{HEMIm}][\text{NTf}_2]$  a stable DLS signal could be observed, in sharp contrast to no signal in  $[\text{C}_1\text{C}_2\text{Im}][\text{NTf}_2]$ . All these facts conclude that the hydroxyl-functionalized IL plays a very important role in the formation of the SA sample.

The aqueous–IL interface is another critical factor for the formation of the SA sample. Two solutions, CMPO and uranyl both dissolved in  $[\text{HEMIm}][\text{NTf}_2]$ , which were pre-equilibrated with 0.1 M  $\text{HNO}_3$ , were mixed together and consequently formed a turbid solution. Only some mesoscopic intermediates instead of a macro SA sample were observed (Fig. S9a, ESI<sup>†</sup>). Nonetheless, with the addition of an equivalent volume of 0.1 M  $\text{HNO}_3$ , an aqueous–IL interface was established, the intermediates started to aggregate immediately and a yellow SA sample appeared at the interface within minutes (Fig. S9b, ESI<sup>†</sup>). In light of this phenomenon, we can assume that due to the traction and local effect of the aqueous–IL interface, these intermediates could move to the interfacial region, and then further aggregate to form the uranium-rich SA sample.

Based on the aforementioned discussion, a potential mechanism for the formation of the macroscopic uranium-rich SA sample could be speculated. The  $\text{UO}_2(\text{CMPO})_3^{2+}$  complex is formed in the aqueous phase, and then extracted in the IL-phase *via* a cation

exchange mechanism. The complex and the cation/anion moieties of the IL started to assemble into intermediates, and further aggregated to form the uranium-rich SA sample at the aqueous–IL interface *via* self-assembly (Fig. 4).

$[\text{HEMIm}][\text{NTf}_2]$  plays a key role in the self-assembly process of the SA sample formation. Its surfactant-like behaviours are quite different from those of the analogues without the hydroxyl-functionalized IL, leading to different interfacial tensions. Besides, the hydroxyl-functionalized IL can participate in the self-assembly process itself, by being incorporated in the final form of the macroscopic assembly. This process does not stop until the extraction equilibrium of uranyl ions is achieved. In this quite delicate process, the hydroxyl-functionalized IL in the interfacial region is consumed continually, and the surface tension gradient is established between the interfacial region and the bulk IL, which in turn drives the cation/anion moieties of the IL together with the uranyl–CMPO complex to be pulled towards the aqueous–IL interface by the Marangoni effect. Self-assembly can then proceed as the intermediates further gather through the electrostatic force,  $\pi$ -stacking, H-bonding and solvophobic interaction,<sup>18,22</sup> forming a uranium-rich macroscopic SA sample spontaneously, till the end of the transformation of uranyl ions into the solid SA sample.

In order to evaluate the recovery of uranium in the aqueous phase from the solid SA sample, more extraction experiments were performed to investigate the effect of the concentration of CMPO (in the IL phase) and that of  $\text{HNO}_3$  (in the aqueous phase) on the equilibrium partitioning of uranium among the three phases (Fig. 5a, b and Table S2, ESI<sup>†</sup>). The partitioning percentage of uranium in the aqueous phase decreases with the molar ratio of the ligand to uranium ( $R$ ) increasing when  $R$  is less than 6, while that in the SA phase increases nearly linearly (Fig. 5a and Fig. S10, ESI<sup>†</sup>); when  $R \geq 6$ , over 99.95% of uranium in the aqueous phase is removed, and the partitioning of uranium between the IL phase and the solid phase is about 5% and 95%, respectively. That is to say, the extracted uranium predominantly accumulates in the SA phase which is easy to be retrieved, hence can avoid the back extraction and stripping steps in traditional extraction systems. Fig. 5b shows that for the  $\text{HNO}_3$  concentration ranging from 0.25 M to 3 M, the acidity of the aqueous phase affects the extraction efficiency little. These experimental results strongly suggest that the designed extraction system is of high extraction efficiency in a wide range of acidity, which can be directly applied in the spent fuel-processing without pH adjustments. The extra benefit of this extraction method is that the IL separated from the aqueous phase after extraction could be reused, so the amount of the radioactive organic waste can be reduced to a great extent. Note that CMPO and the IL are both consumed due to the formation of the SA sample, so for the extraction in 2nd and 3rd cycles, additional ligands in the new IL are added to compensate the loss (see detailed Experimental conditions in Tables S3 and S4, ESI<sup>†</sup>). As illustrated in Fig. 5c, the contents of uranium in the aqueous phase and in the IL phase are almost identical to those after the 1st run, while a slight increase in the SA phase occurs. Since 5% of initial uranium is retained in the IL phase in the 1st run due to the distribution equilibrium, the recovery of uranium from aqueous solution to the solid phase in the 2nd and

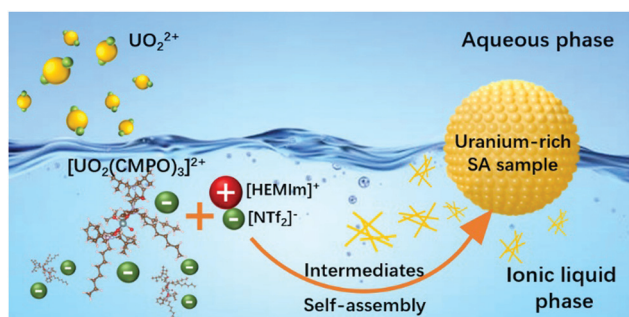


Fig. 4 The potential formation mechanism for the macroscopic uranium-rich SA sample.

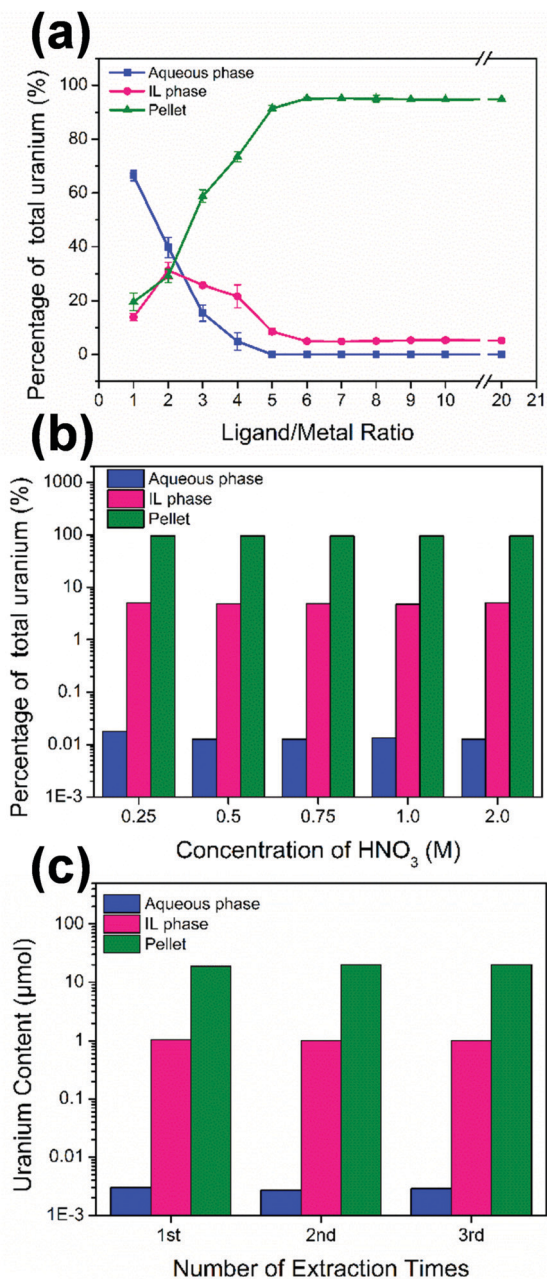


Fig. 5 The extraction efficiency of uranium under different conditions: (a) with various ligand/uranium ratios, (b) at various concentrations of HNO<sub>3</sub>, and (c) with the reused IL.

3rd cycles is nearly 100% with the reused IL which already contains a small amount of uranium, and therefore the content of uranium in the solid phase increases.

In summary, our designed extraction system based on self-assembly displays efficiency, cleanliness, reusability and overcomes the drawbacks of the conventional solvent extraction systems. Moreover, this separation strategy can be used for the recovery of many other metals such as iron, copper, zinc, gold, manganese, lead, vanadium and aluminum (Fig. S11, ESI<sup>†</sup>), making it a promising method in mining and treatment of heavy metal-containing waste water. It is worth pointing out that when this

strategy is applied to the extraction of lanthanide ions (Nd<sup>3+</sup>, Eu<sup>3+</sup>, Dy<sup>3+</sup> and Er<sup>3+</sup>), complexes of lanthanide ions cannot form the macroscopic solid SA sample (Fig. S12, ESI<sup>†</sup>). It is a positive observation and we should conduct research in the future. Additionally, this process enables a metal complex to assemble from the microscopic scale to the mesoscopic scale and then to the macroscopic scale *via* the Marangoni effect in a simple system continuously and spontaneously, overcoming some long-lasting difficulties with driving forces, hence may promote the development of supramolecular assembly both in mechanism and application.

All experimental data and the structure of the referred ILs and CMPO, relevant to this communication, have been reported in the ESI<sup>†</sup>.

This work was financially supported by the National Natural Science Foundation of China (Grant No. U1830202 and 11675156) and the Science Challenge Project (TZ2016004). The authors thank Lili Luo for assistance with SEM experiments. Uranium concentration measurements were carried out with help from Liangang Zhuo. The authors also acknowledge Rende Ze for his effort in video making.

## Conflicts of interest

There are no conflicts of interest to declare.

## Notes and references

- X. Sun, H. Luo and S. Dai, *Chem. Rev.*, 2012, **112**, 2100–2128.
- C. W. Abney, R. T. Mayes, T. Saito and S. Dai, *Chem. Rev.*, 2017, **117**, 13935–14013.
- S. Ma, L. Huang, L. Ma, Y. Shim, S. M. Islam, P. Wang, L.-D. Zhao, S. Wang, G. Sun, X. Yang and M. G. Kanatzidis, *J. Am. Chem. Soc.*, 2015, **137**, 3670–3677.
- L. Ling and W.-x. Zhang, *J. Am. Chem. Soc.*, 2015, **137**, 2788–2791.
- M.-L. Feng, D. Sarma, X.-H. Qi, K.-Z. Du, X.-Y. Huang and M. G. Kanatzidis, *J. Am. Chem. Soc.*, 2016, **138**, 12578–12585.
- D. Beltrami, G. Cote, H. Mokhtari, B. Courtaud, B. A. Moyer and A. Chagnes, *Chem. Rev.*, 2014, **114**, 12002–12023.
- R. J. Ellis and M. R. Antonio, *Langmuir*, 2012, **28**, 5987–5998.
- S. Gao, T. Sun, Q. Chen and X. Shen, *Radiochim. Acta*, 2016, **104**, 457.
- M.-J. Cheng, Q. Zhang and F. Shi, *Chin. J. Polym. Sci.*, 2017, **36**, 306–321.
- A. Harada, R. Kobayashi, Y. Takashima, A. Hashidzume and H. Yamaguchi, *Nat. Chem.*, 2010, **3**, 34.
- M. Nakahata, Y. Takashima and A. Harada, *Angew. Chem., Int. Ed.*, 2014, **53**, 3617–3621.
- M. Cheng, F. Shi, J. Li, Z. Lin, C. Jiang, M. Xiao, L. Zhang, W. Yang and T. Nishi, *Adv. Mater.*, 2014, **26**, 3009–3013.
- Q. Zhang, C. Liu, G. Ju, M. Cheng and F. Shi, *Macromol. Rapid Commun.*, 2018, **39**, 1800180.
- M. Cheng, G. Zhu, L. Li, S. Zhang, D. Zhang, A. J. C. Kuehne and F. Shi, *Angew. Chem., Int. Ed.*, 2018, **57**, 14106–14110.
- H. Zhang, W. Duan, L. Liu and A. Sen, *J. Am. Chem. Soc.*, 2013, **135**, 15734–15737.
- L. A. Blanchard, D. Hancu, E. J. Beckman and J. F. Brennecke, *Nature*, 1999, **399**, 28.
- J. E. Bara, D. E. Camper, D. L. Gin and R. D. Noble, *Acc. Chem. Res.*, 2010, **43**, 152–159.
- K. Dong, X. Liu, H. Dong, X. Zhang and S. Zhang, *Chem. Rev.*, 2017, **117**, 6636–6695.
- M. H. Mallah, F. Shemirani and M. G. Maragheh, *Environ. Sci. Technol.*, 2009, **43**, 1947–1951.
- K. Shimojo, K. Kurahashi and H. Naganawa, *Dalton Trans.*, 2008, 5083–5088.
- A. S. Pensado, M. F. C. Gomes, J. N. C. Lopes, P. Malfreyt and A. A. H. Pádua, *Phys. Chem. Chem. Phys.*, 2011, **13**, 13518–13526.